Progress In Electromagnetics Research, Vol. 137, 293–309, 2013

AN EFFICIENT SAR JAMMER WITH DIRECT RADIO FREQUENCY PROCESSING (DRFP)

Qingfu Liu*, Jian Dong, Xuesong Wang, Shiqi Xing, and Bo Pang

School of Electronic Science and Engineering, National University of Defense Technology, Changsha 410073, China

Abstract—DRFM (Digital Radio Frequency Memory) is now widely utilized by modern radar jammers due to its high efficiency in jamming generation. However, its jammer structure is somewhat complex, since the up-conversion and down-conversion processes must be included. This paper proposes a new Synthetic Aperture Radar (SAR) jammer architecture utilizing Direct Radio Frequency Processing (DRFP), wherein both the up-conversion and down-conversion modules can be excluded. DRFP has a very compact hardware structure which employs Direct Digital Synthesizer (DDS), phase shifter, and delay lines for jamming modulation. Finally, the performances of DRFP are shown by both the inner-field test and a rail-way SAR experiment to be rather effective in jamming generation.

1. INTRODUCTION

With a history as long as half a century, Synthetic Aperture Radar (SAR) has become a very effective tool for city planning [1], environmental monitoring [2], Foreign Object Detection (FOD) [3], and man-made target detection and recognition [4–6]. Due to its outstanding imaging performance, SAR has been widely utilized in warfare surveillance. Accordingly, SAR Electronic Counter Measures (ECM) is also a hot topic nowadays. According to the relationship between SAR transmitted signal and its jamming, SAR ECM technologies can be divided into three types [7–9], i.e., non-coherent jamming, partially coherent jamming, and coherent jamming. Non-coherent jamming [10, 11] is easiest to be designed, but needs largest

Received 21 September 2012, Accepted 21 November 2012, Scheduled 21 February 2013
* Corresponding author: Qingfu Liu (liu_675675@163.com).

transmit power and is most susceptible to the detection of SAR receiver. It can be cancelled through a number of Electronic Counter-Counter Measures (ECCM) techniques, e.g., wideband sidelobe-cancellation [12], spatial filtering [13] and adaptive beamforming [14]. The partially coherent jamming [15, 16] needs modest transmit power. But it can still be easily detected by SAR and then be cancelled by the ECCM technologies. The coherent jamming [7, 17] needs smallest transmit power and can generate false targets in SAR image with similar properties of the real targets. So this kind of jamming can not be easily detected by SAR receiver and it will become the main development direction of SAR ECM.

Generally, the generation of coherent jamming needs to precisely estimate the parameters of SAR transmitted signal, which are often difficult to be derived in high precisions. So a jammer utilizing the coherent jamming is generally difficult to be designed and costly [7, 9]. To generate coherent jamming with arbitrary modulations, DRFM (Digital Radio Frequency Memory) is now widely utilized by modern jammer, where both the down-conversion and up-conversion processes are needed. In this paper, we propose a more efficient jammer based on Direct Radio Frequency Processing (DRFP), who utilizes Direct Digital Synthesizer (DDS), phase shifter, and delay lines for jamming modulation. The merit of DRFP is no need of the down-conversion and up-conversion processes, and its hardware structure is much compact than that of DRFM. Furthermore, a DRFP enjoys smaller jammer hardware delay owning to its compact structure, which is critical for SAR decoy generation.

2. THE PRINCIPLES OF DRFP

The working processes of a typical DRFM-based jammer can be described as follows. Firstly, the jammer receives and detects the SAR transmitted signal. Secondly, the jammer down-converts the received SAR signal and estimates the parameters of SAR signal. Thirdly, the jammer modulates the down-converted SAR signal according to the estimated parameters. Fourthly, the jammer up-converts the modulated signal (i.e., the jamming) and then transmits it back to SAR receiver. Finally, the jamming is added upon the echoes of real targets and is processed by SAR imaging. To illustrate the principles of DRFP in a clearer manner, the SAR jamming without any modulation is introduced in the first part of this section.

2.1. SAR Jamming without Any Modulation

The SAR signal received by jammer after down-conversion can be expressed as

$$s_{\mathrm{SAR}}(\tau,\eta) = A_0 w_\tau\left(\tau - \frac{R(\eta)}{c}\right) w_\eta(\eta-\eta_c)\exp\left\{j2\pi f_c\left(\tau-\frac{R(\eta)}{c}\right)\right\} \times \exp\left\{j\pi K_\eta\left(\tau-\frac{R(\eta)}{c}\right)^2\right\} \quad (1)$$

where τ and η denote the fast-time and slow-time, respectively. $w_\tau(g)$ and $w_\eta(g)$ are the windowing functions in fast-time and slow-time, respectively. $j=\sqrt{-1}$. f_c is the carrier frequency of SAR transmitted signal. c is the velocity of light. η_c is the slow-time when SAR is closest to the jammer in slant range. K_η is the chirp rate of Linear Frequency Modulation (LFM). $R(\eta)$ is the slant range defined as

$$R(\eta) = \sqrt{R_{\min}^2 + v_\eta^2\eta^2} \quad (2)$$

$R_{\min}$ is the minimum slant range between SAR and jammer. v_η is the velocity of SAR platform. If the jammer transmit back the received SAR signal without any extra modulation, then the jamming received by SAR receiver is a two-way delayed version of SAR transmitted signal (see (1)), that is

$$s_{\mathrm{jamming}}(\tau,\eta) = A_1 w_\tau\left(\tau - \frac{2R(\eta)}{c}\right) w_\eta(\eta-\eta_c)\exp\left\{j2\pi f_c\left(\tau-\frac{2R(\eta)}{c}\right)\right\} \times \exp\left\{j\pi K_\eta\left(\tau-\frac{2R(\eta)}{c}\right)^2\right\} \quad (3)$$

where A_1 is the amplitude of jamming. Obviously, (3) has a similar expression to the echo of point-like target. So its imaging result is also similar to that of the point-like target and can be written as

$$s_{\mathrm{imaging}}(\tau,\eta) = A_{\mathrm{imaging}}\mathrm{sinc}\left(\frac{\tau-2R_{\min}/c}{\rho_\tau}\right)\mathrm{sinc}\left(\frac{\eta-\eta_c}{\rho_\eta}\right) \quad (4)$$

where $\mathrm{sinc}(g)$ is sinc function defined as

$$\mathrm{sinc}(x) = \frac{\sin(\pi x)}{\pi x} \quad (5)$$

A_{imaging} is the amplitude of imaging result. ρ_τ and ρ_η are the resolutions in range-direction and azimuth-direction, respectively. They can be expressed as

$$\begin{cases} \rho_\tau \approx \frac{1}{K_\tau T_p} = \frac{1}{B_\tau} \\ \rho_\eta \approx \frac{\lambda_c}{2\theta_{\mathrm{az}} v_\eta} = \frac{1}{B_\eta} \end{cases} \quad (6)$$

where T_p is the pulse width of LFM. λ_c is the wave length of SAR transmitted signal; θ_{az} is SAR beam width in azimuth direction. B_η is the Doppler bandwidth. It can be seen from (4) that, the imaging result of this jamming is similar to that of point-like target. The mainlobe widths (i.e., the resolutions for target) in range-direction and azimuth-direction are determined by the chirp bandwidth and Doppler bandwidth, respectively (see (6)).

2.2. DRFP with Periodic Modulation Waveforms

The basic principles of periodic modulated jamming have been thoroughly discussed in [7]. This kind of jamming has the ability to generate grid-like decoys in SAR image and has been proved to be very effective. However, [7] utilizes the DRFM structure to perform the periodic modulation, which will induce the jammer hardware structure to be somewhat complex. In the following part of this section, a new jammer structure utilizing DRFP is proposed and both down-conversion and up-conversion modules are no longer needed. Since no down-conversion is needed, the SAR signal received by jammer should be expressed in a form of Radio Frequency (RF) as

$$s_{\mathrm{SAR}}(\tau,\eta) = A_0 w_\tau\left(\tau-\frac{R(\eta)}{c}\right) w_\eta(\eta-\eta_c)\sin\left[2\pi f_c\left(\tau-\frac{R(\eta)}{c}\right)\right] \times \sin\left[\pi K_\eta\left(\tau-\frac{R(\eta)}{c}\right)^2\right] \tag{7}$$

Comparing (1) with (7), it can be seen that (1) is the down-converted version of (7). In order to modulate the received SAR signal in slow-time, a phase shifter is utilized by DRFP to shift the phases to introduce phase modulation for different pulses. After the modulation of phase shifter, (7) should be expressed as

$$s_{\mathrm{az}}(\tau,\eta) = A_0 w_\tau\left(\tau-\frac{R(\eta)}{c}\right) w_\eta(\eta-\eta_c)\sin\left[2\pi f_c\left(\tau-\frac{R(\eta)}{c}\right)+\varphi_{\mathrm{peri}}(\eta)\right] \times \sin\left[\pi K_\eta\left(\tau-\frac{R(\eta)}{c}\right)^2\right] \tag{8}$$

where $\varphi_{\mathrm{peri}}(\eta)$ is a periodic phase function with respect to the slow-time η. Also, the fast-time modulation of DRFP is conducted in RF and a periodic signal generated by DDS is used as the modulation waveform. After the fast-time modulation of (8), the signal model of

DRFP should be written as

$$s_{\mathrm{DRFP}}(\tau,\eta)=A_0 w_\tau\left(\tau-\frac{R(\eta)}{c}\right)w_\eta(\eta-\eta_c)\sin\left[2\pi f_c\left(\tau-\frac{R(\eta)}{c}\right)+\varphi_{\mathrm{peri}}(\eta)\right]\times\sin\left[\pi K_\eta\left(\tau-\frac{R(\eta)}{c}\right)^2\right]gm_{\mathrm{peri}}\left(\tau-\frac{R(\eta)}{c}\right) \quad (9)$$

where $m_{\mathrm{peri}}(\tau)$ is a periodic function with respect to the fast-time τ. Then the jammer transmits the signal expressed in (9) back to SAR receiver and the DRFP jamming received by SAR can be expressed as

$$s_{\mathrm{DRFP}}(\tau,\eta)=A_{\mathrm{jamming}}w_\tau\left(\tau-\frac{2R(\eta)}{c}\right)w_\eta(\eta-\eta_c)\sin\left[2\pi f_c\left(\tau-\frac{2R(\eta)}{c}\right)+\varphi_{\mathrm{peri}}(\eta)\right]\times\sin\left[\pi K_\eta\left(\tau-\frac{2R(\eta)}{c}\right)^2\right]gm_{\mathrm{peri}}\left(\tau-\frac{2R(\eta)}{c}\right) \quad (10)$$

Before SAR imaging process, DRFP in (10) is down-converted by SAR receiver to derive its base band form as

$$\begin{aligned}
&s_{\mathrm{DRFP}}(\tau,\eta)\\
&=A_{\mathrm{jamming}}w_\tau\left(\tau-\frac{2R(\eta)}{c}\right)w_\eta(\eta-\eta_c)\exp\left\{j2\pi f_c\left(\tau-\frac{2R(\eta)}{c}\right)\right.\\
&\quad\left.+j\varphi_{\mathrm{peri}}(\eta)\right\}\times\exp\left\{j\pi K_\eta\left(\tau-\frac{2R(\eta)}{c}\right)^2\right\}gm_{\mathrm{peri}}\left(\tau-\frac{2R(\eta)}{c}\right)\\
&=A_{\mathrm{jamming}}w_\tau\left(\tau-\frac{2R(\eta)}{c}\right)w_\eta(\eta-\eta_c)\exp\left\{j2\pi f_c\left(\tau-\frac{2R(\eta)}{c}\right)\right\}\\
&\quad\times\exp\left\{j\pi K_\eta\left(\tau-\frac{2R(\eta)}{c}\right)^2\right\}g\exp\{j\varphi_{\mathrm{peri}}(\eta)\}\,m_{\mathrm{peri}}\left(\tau-\frac{2R(\eta)}{c}\right)
\end{aligned} \quad (11)$$

In fact, SAR imaging can be factored into two separate parts after range cell migration correction (RCMC) due to the vast differences between fast-time and slow-time. Thus (11) after RCMC can be rewritten as

$$s_{\mathrm{DRFP}}(\tau,\eta)=s_{\mathrm{DRFP\text{-}}\tau}(\tau)\times s_{\mathrm{DRFP\text{-}}\eta}(\eta) \quad (12)$$

where $s_{\mathrm{DRFP\text{-}}\tau}(\tau)$ and $s_{\mathrm{DRFP\text{-}}\eta}(\eta)$ represent the fast-time and slow-time components of DRFP jamming, respectively. And they can be expressed as

$$\begin{cases}
s_{\mathrm{DRFP\text{-}}\tau}(\tau)=A_{\mathrm{jamming}}w_\tau(\tau)\exp\left\{j\pi K_\eta\tau^2\right\}gm_{\mathrm{peri}}(\tau)\\
s_{\mathrm{DRFP\text{-}}\eta}(\eta)=w_\eta(\eta-\eta_c)\exp\left\{-j4\pi\frac{f_cR(\eta)}{c}\right\}g\exp\{j\varphi_{\mathrm{peri}}(\eta)\}
\end{cases} \quad (13)$$

Note that $s_{\text{DRFP-}\tau}(\tau)$ and $s_{\text{DRFP-}\eta}(\eta)$ in (12) are independent from each other. So the imaging result of DRFP is equal to the multiplication of $s_{\text{DRFP-}\tau}(\tau)$ and $s_{\text{DRFP-}\eta}(\eta)$'s imaging results. That is, the imaging results of (12) can be expressed as

$$\begin{aligned} s_{\text{DRFP}}^{\text{image}}(\tau,\eta) &= \aleph\left[s_{\text{DRFP-}\tau}(\tau) \times s_{\text{DRFP-}\eta}(\eta)\right] \\ &= \aleph\left[s_{\text{DRFP-}\tau}(\tau)\right] \times \aleph\left[s_{\text{DRFP-}\eta}(\eta)\right] \\ &= \hat{s}_{\text{DRFP-}\tau}^{\text{image}}(\tau) \times s_{\text{DRFP-}\eta}^{\text{image}}(\eta) \end{aligned} \tag{14}$$

where $\aleph(g)$ denotes SAR imaging operator. The superscript "image" denotes the corresponding imaging result. To facilitate the analysis in the following part, the modulation function in (13) should be rewritten in another form as

$$\begin{cases} m_{\text{peri}}(\tau) = m_0(\tau) \otimes_\tau \delta_{T_\tau}(\tau) \\ \exp\{j\varphi_{\text{peri}}(\eta)\} = \varphi_0(\eta) \otimes_\eta \delta_{T_\eta}(\eta) \end{cases} \tag{15}$$

where $\otimes_\tau$ and $\otimes_\eta$ denote convolutions with respect to fast-time and slow-time, respectively. $m_0(\tau)$ and $\varphi_0(\eta)$ are the main periods of the modulation waveforms with periods of $T_{\tau 0}$ and $T_{\eta 0}$ in fast-time and slow-time, respectively. $\delta_{T_\tau}(\tau)$ and $\delta_{T_\eta}(\eta)$ are the periodic Dirac functions defined as

$$\begin{cases} \delta_{T_{\tau 0}}(\tau) = \sum\limits_{n=-\infty}^{+\infty} \delta(\tau - nT_{\tau 0}) \\ \delta_{T_{\eta 0}}(\eta) = \sum\limits_{l=-\infty}^{+\infty} \delta(\eta - lT_{\eta 0}) \end{cases} \tag{16}$$

The Fourier Transform (FT) of (16) can be expressed as

$$\begin{cases} \delta_{f_{\tau 0}}(f_\tau) = \text{FT}\left[\delta_{T_{\tau 0}}(\tau)\right] = f_{\tau 0} \sum\limits_{n=-\infty}^{+\infty} \delta(f_\tau - nf_{\tau 0}) \\ \delta_{f_{\eta 0}}(f_\eta) = \text{FT}\left[\delta_{T_{\eta 0}}(\eta)\right] = f_{\eta 0} \sum\limits_{l=-\infty}^{+\infty} \delta(f_\eta - lf_{\eta 0}) \end{cases} \tag{17}$$

where the operator FT[g] denotes FT. f_τ and f_η are range-frequency and azimuth-frequency, respectively. $f_{\tau 0} = T_{\tau 0}^{-1}$ and $f_{\eta 0} = T_{\eta 0}^{-1}$. Substituting (15) into (13) yields

$$\begin{cases} s_{\text{DRFP-}\tau}(\tau) = A_{\text{jamming}} w_\tau(\tau) \exp\left\{j\pi K_\eta \tau^2\right\} g m_0(\tau) \otimes_\tau \delta_{T_{\tau 0}}(\tau) \\ s_{\text{DRFP-}\eta}(\eta) = w_\eta(\eta - \eta_c) \exp\left\{-j4\pi \frac{f_c R(\eta)}{c}\right\} g\varphi_0(\eta) \otimes_\eta \delta_{T_{\eta 0}}(\eta) \end{cases} \tag{18}$$

According to the well-known property of FT, convolution in the time domain is equivalent to multiplication in the frequency domain,

and multiplication in the time domain is equivalent to convolution in the frequency domain. That is, FT of (18) can be expressed as

$$\begin{cases} S_{\text{DRFP-}\tau}(f_\tau) = S_\tau(f_\tau) \otimes_{f_\tau} [M_0(f_\tau)\,\delta_{f_{\tau 0}}(f_\tau)] \\ S_{\text{DRFP-}\eta}(f_\eta) = S_\eta(f_\eta) \otimes_{f_\eta} \left[\Phi_0(f_\eta)\,\delta_{f_{\eta 0}}(f_\eta)\right] \end{cases} \tag{19}$$

where $\otimes_{f_\tau}$ and $\otimes_{f_\eta}$ represent convolution with respect to range-frequency f_τ and azimuth-frequency f_η, respectively. $M_0(f_\tau)$ and $\Phi_0(f_\eta)$ are FTs of $m_0(\tau)$ and $\varphi_0(\eta)$, respectively. And

$$\begin{cases} S_\tau(f_\tau) = \text{FT}\left[A_{\text{jamming}} w_\tau(\tau) \exp\left\{j\pi K_\eta \tau^2\right\}\right] \\ S_\eta(f_\eta) = \text{FT}\left[w_\eta(\eta-\eta_c) \exp\left\{-j4\pi \frac{f_c R(\eta)}{c}\right\}\right] \end{cases} \tag{20}$$

Substituting (17) into the terms in right sides of the convolutions to get

$$\begin{cases} M_0(f_\tau)\,\delta_{f_{\tau 0}}(f_\tau) = M_0(f_\tau)\, f_{\tau 0} \sum\limits_{n=-\infty}^{+\infty} \delta(f_\tau - n f_{\tau 0}) \\ \qquad\qquad = \sum\limits_{n=-\infty}^{+\infty} f_{\tau 0} M_0(n f_{\tau 0})\,\delta(f_\tau - n f_{\tau 0}) \\ \Phi_0(f_\eta)\,\delta_{f_{\eta 0}}(f_\eta) = \Phi_0(f_\eta)\, f_{\eta 0} \sum\limits_{l=-\infty}^{+\infty} \delta(f_\eta - l f_{\eta 0}) \\ \qquad\qquad = \sum\limits_{l=-\infty}^{+\infty} f_{\eta 0} \Phi_0(l f_{\eta 0})\,\delta(f_\eta - l f_{\eta 0}) \end{cases} \tag{21}$$

Substituting (21) into (19) yields

$$\begin{cases} S_{\text{DRFP-}\tau}(f_\tau) = \sum\limits_{n=-\infty}^{+\infty} f_{\tau 0} M_0(n f_{\tau 0})\, S_\tau(f_\tau - n f_{\tau 0}) \\ S_{\text{DRFP-}\eta}(f_\eta) = \sum\limits_{l=-\infty}^{+\infty} f_{\eta 0} \Phi_0(l f_{\eta 0})\, S_\eta(f_\eta - l f_{\eta 0}) \end{cases} \tag{22}$$

The Inverse Fourier Transform (IFT) of (22) can be written as

$$\begin{cases} s_{\text{DRFP-}\tau}(\tau) = \sum\limits_{n=-\infty}^{+\infty} f_{\tau 0} M_0(n f_{\tau 0})\, s_\tau(\tau) \exp\{j2n\pi f_{\tau 0}\tau\} \\ s_{\text{DRFP-}\eta}(\eta) = \sum\limits_{l=-\infty}^{+\infty} f_{\eta 0} \Phi_0(l f_{\eta 0})\, s_\eta(\eta) \exp\{j2l\pi f_{\eta 0}\tau\} \end{cases} \tag{23}$$

Therefore, DRFP can be deemed as the superposition of Single Tone Modulated Jamming (STMJ). Then the imaging results of (23)

can be expressed as

$$\begin{cases} \hat{s}^{\text{image}}_{\text{DRFP-}\tau}(\tau) = \sum\limits_{n=-\infty}^{+\infty} f_{\tau 0} M_0(n f_{\tau 0}) \operatorname{sinc}\left(\frac{\tau - 2R_{\min}/c - n f_{\tau 0}/K_\tau}{\rho_\tau} \frac{B_\tau - |n f_{\tau 0}|}{B_\tau}\right) \\ \qquad\qquad |n| \le \frac{B_\tau}{|f_{\tau 0}|} \\ s^{\text{image}}_{\text{DRFP-}\eta}(\eta) = \sum\limits_{l=-\infty}^{+\infty} f_{\eta 0} \Phi_0(l f_{\eta 0}) \operatorname{sinc}\left(\frac{\eta - l f_{\eta 0}/K_\eta}{\rho_\eta} \frac{B_\eta - |l f_{\eta 0}|}{B_\eta}\right) \\ \qquad\qquad |l| \le \frac{B_\eta}{|f_{\eta 0}|} \end{cases} \tag{24}$$

By substituting (24) into (14), the imaging result of DRFP can be derived as

$$\begin{aligned} & s^{\text{image}}_{\text{DRFP}}(\tau, \eta) \\ &= \sum_{n=-\infty}^{+\infty} f_{\tau 0} M_0(n f_{\tau 0}) \operatorname{sinc}\left(\frac{\tau - 2R_{\min}/c - n f_{\tau 0}/K_\tau}{\rho_\tau} \frac{B_\tau - |n f_{\tau 0}|}{B_\tau}\right) \\ &\quad \times \sum_{l=-\infty}^{+\infty} f_{\eta 0} \Phi_0(l f_{\eta 0}) \operatorname{sinc}\left(\frac{\eta - l f_{\eta 0}/K_\eta}{\rho_\eta} \frac{B_\eta - |l f_{\eta 0}|}{B_\eta}\right) \\ &\qquad\qquad |n| \le \frac{B_\tau}{|f_{\tau 0}|} \text{ and } |l| \le \frac{B_\eta}{|f_{\eta 0}|} \end{aligned} \tag{25}$$

Until now, we have derived the imaging results of DRFP with periodic modulation waveforms. As shown in (25), DRFP also has the ability to generate grid-like false targets. The intervals between two adjacent points are in inverse proportion to the periods of DRFP's modulation waveform for both range-direction and azimuth-direction, whereas the numbers of peaks are proportional to the periods of DRFP's modulation waveform. The lobe widths of peaks are proportional to $B_\tau / (B_\tau - |n f_{\tau 0}|)$ and $B_\eta / (B_\eta - |l f_{\eta 0}|)$ in range-direction and azimuth-direction, respectively. Comparing (25) with the results represented by [7], one can find that both DRFP-based and DRFM-based jamming have similar imaging output. That is, DRFP can achieve similar performance of DRFM but has a more simplified jammer structure, owning to its direct modulation in RF.

2.3. DRFP Utilizing Only Fast-time Modulation Waveform

Two-dimensional periodic modulations are utilized by the DRFP discussed in last sub-section, where a phase shifter and a DDS are needed. To further simplify the structure of DRFP based jammer, the phase shifter is excluded in the following jamming generation. And we are trying to use only a DDS to generate the desired DRFP jamming, where the coupling between fast-time and slow-time of SAR

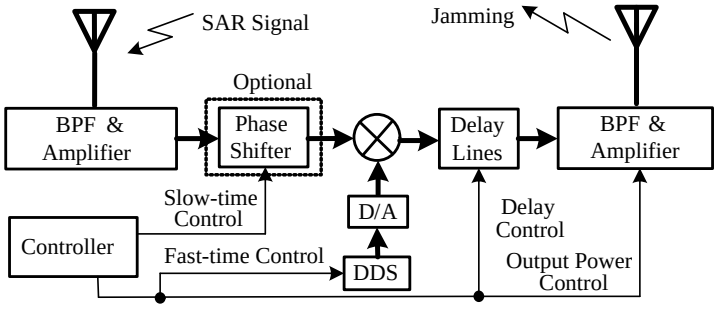

Figure 1. The structure of DRFP-based jammer.

are considered. As having been demonstrated by [7], the modulations in fast-time can introduce extra modulations in slow-time. Appendix A gives three typical modulations utilized by DRFP, and to be concise, their corresponding results are not discussed here.

2.4. The DRFP Hardware Structure

The jamming generation procedure of DRFP can be described as follows. Firstly, the SAR transmitted signal is received, band-filtered, and amplified by the jammer. Secondarily, the signal is phase-shifted according to the slow-time modulation waveform of DRFP. Thirdly, the phase-shifted signal is further multiplied by a fast-time modulation waveform generated by DDS. Fourthly, the modulated signal (i.e., jamming) is divided into multiple delay groups to forge multi-blocks of jamming. Finally, the jamming is filtered, amplified, and transmitted by the jammer. As discussed above, the function of the phase shifter can be replaced by the control of initial phase modulation of DDS generated waveforms. Thus the phase shifter is optional here. In real applications, the carrier frequency of SAR transmitted signal is much higher than the highest frequency of jamming modulation waveform. So both the DDS and Digital-to-Analogue (D/A) can work at intermediate frequency with relatively lower data rate.

3. EXPERIMENTS AND ANALYSIS

3.1. Inner Field Test

Before the rail-way SAR experiments, the performances of DRFP jammer are tested by an Inner Field SAR Simulator (IFSARS). The whole test procedures can be described as follows. Firstly, the output of IFSARS is connected with the input of DRFP jammer, and the

input of IFSARS is connected with the output of DRFP jammer; Secondly, the parameters of IFSARS are set in accordance with the real SAR systems to be simulated; Thirdly, IFSARS transmits its simulated SAR signal to DRFP jammer. Then DRFP jammer receives the simulated SAR signal and estimates the parameters of the signal; Fourthly, the jammer generates the jamming according to its estimated SAR signal parameters, and transmits the jamming back to IFSARS. Finally, IFSARS receives the jamming, processes it with SAR imaging algorithm, and analyzes the performances of DRFP jammer.

In our experiments, six DRFP jammings with different modulations are tested. Their corresponding test results are shown in Fig. 2

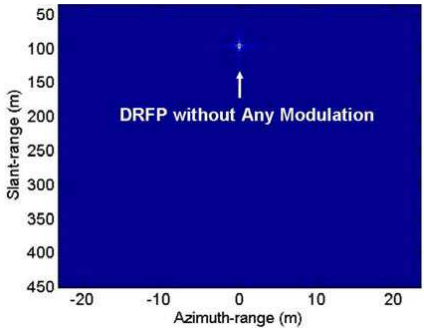

Figure 2. DRFP without any modulation. (Horizontal: Azimuth-direction; Vertical: Range-direction).

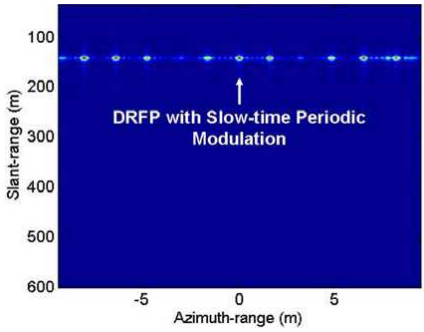

Figure 3. DRFP with slow-time periodic modulation. (Horizontal: Azimuth-direction; Vertical: Range-direction).

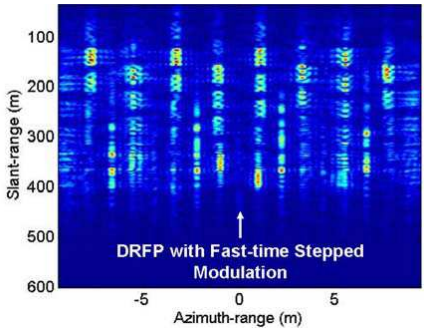

Figure 4. DRFP with fast-time stepped modulation. (Horizontal: Azimuth-direction; Vertical: Range-direction).

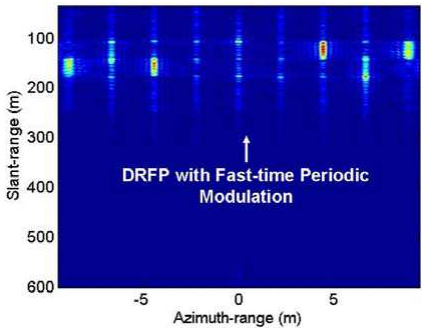

Figure 5. DRFP with fast-time periodic modulation. (Horizontal: Azimuth-direction; Vertical: Range-direction).

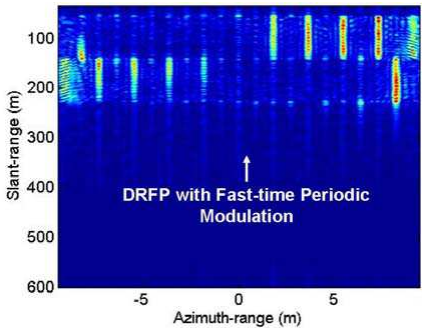

Figure 6. DRFP with fast-time periodic modulation. (Horizontal: Azimuth-direction; Vertical: Range-direction).

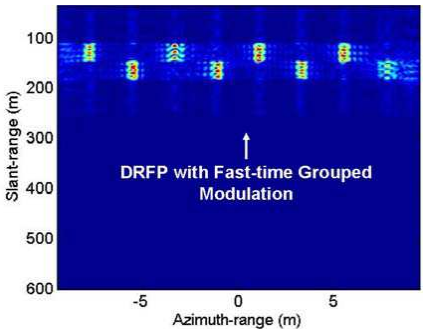

Figure 7. DRFP with fast-time grouped modulation. (Horizontal: Azimuth-direction; Vertical: Range-direction).

to Fig. 6. It can be seen that the imaging result of DRFP without any modulation is a single point (shown in Fig. 2). The imaging result of DRFP with slow-time periodic modulation is a serial of discrete points distributed along azimuth-direction (shown in Fig. 3). With stepped modulation in fast time, DRFP is able to generate multi-blocks within a designated area (shown in Fig. 4). By utilizing fast-time periodic modulation and grouped modulation, multi-line false target can be produced by DRFP (shown in Fig. 5 to Fig. 7).

3.2. Rail-way SAR Experiments

A SAR ECM experiment is conducted by utilizing the rail-way SAR system, developed by National University of Defense Technology (NUDT). The parameters of the railway SAR system are listed in Table 1.

Two trihedrals, within the same slant-range bin of 75 m, are put in the imaging scene (shown in Fig. 8). The minimum slant range of jammer is about 70 m. Firstly, the scene is imaged by the railway SAR without any jamming for the purpose of comparison with the aftermentioned jammed ones. The imaging result of the scene is shown in Fig. 9, where only two trihedrals can be found due to their relatively large RCS. Secondly, by utilizing the slow-time periodic modulation, a line with discrete points along azimuth-direction is generated by DRFP (shown in Fig. 10). It can be deduced from the parameters listed in Table 1 that, the slow-time chirp rate of jammer is about 0.2381 Hz/s. Since the slow-time period of DRFP's modulation waveform is 2.1 s, the interval between two adjacent points of the jamming is about

Table 1. The main parameters of the rail-way SAR.

Carrier frequency	10.48 GHz	**Polarization**	VV
Pulse width	2 μs	**Rail-way velocity**	0.5 m/s
Bandwidth	35 MHz	**Azimuth beamwidth**	3 degrees
Sign of the chirp	positive	**Height of the railway**	3 m
PRF	50 Hz	**Squint angle**	0 degree
Peak transmitted power	45 dBmW	**Sampling rate in fast time**	200 MSamples/s

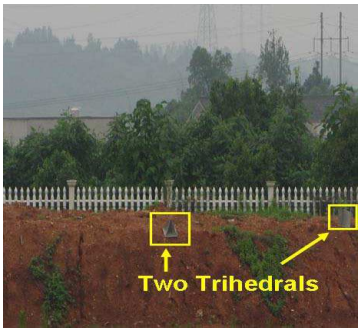

Figure 8. SAR imaging scene.

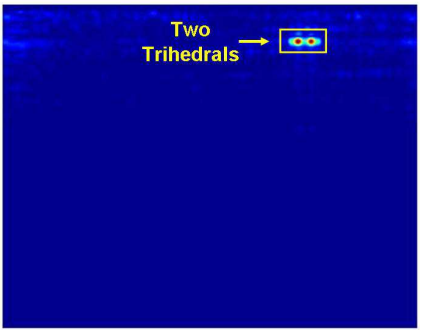

Figure 9. SAR imaging results without jamming.

1 m. Thirdly, multi-line with discrete points along azimuth-direction (i.e., grid-like false target) is generated by DRFP with both slow-time periodic modulation and multi-delay modulation (shown in Fig. 11). The distribution of the jamming can be easily extended by multi-delay modulation, where both delay interval and the number of delays can be controlled by the jammer. However, the transmit power of the jammer was somehow reduced during this experiment scenario, so the imaging result of the jamming can not be observed clearly. Fourthly, four blocks are produced by DRFP with fast-time stepped modulation (shown in Fig. 12). Due to the nonzero start frequency of stepped modulation in both directions, a gap can be seen in the middle of the jamming. Finally, four separate lines along the range-direction are produced by DRFP with fast-time periodic modulation (shown in Fig. 13). Also, because of the nonzero start frequency, a gap can be

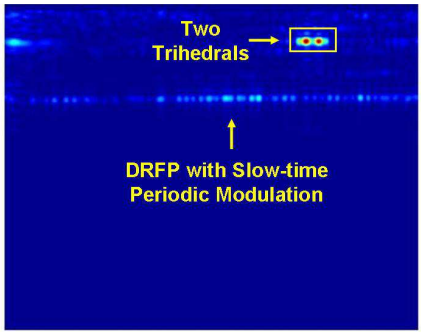

Figure 10. SAR imaging result of DRFP with slow-time periodic modulation.

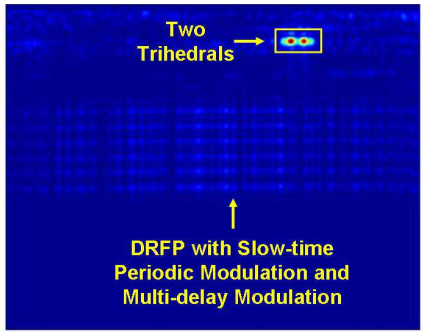

Figure 11. SAR imaging result of DRFP with slow-time periodic modulation and multi-delay modulation.

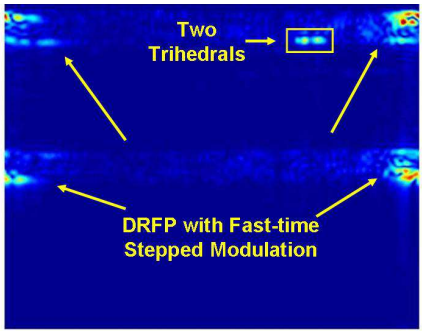

Figure 12. SAR imaging result of DRFP with fast-time stepped modulation.

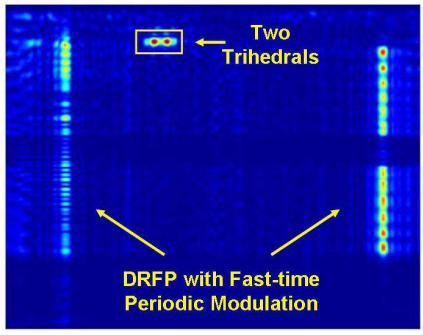

Figure 13. SAR imaging result of DRFP with fast-time periodic modulation

found in the middle of jamming in range direction. Therefore, DRFP is able to generate line-like, grid-like and block-like false targets for SAR image. It is also beneficial to compare the experiment result of DRFP with that of DRFM represented in [1] to come to the conclusion that, both two modulation methods have similar imaging results although the former has a much simplified jammer hardware structure.

4. CONCLUSIONS

A compact and easy-to-be-designed SAR jammer was developed in this paper, where only a DDC and a digital controllable phase shifter are needed for jamming modulation. Compared with the DRFM based

jammer structure, this kind of jammer has a much simplified structure, since both down-conversion and up-conversion modules of the jammer can be removed in the new jammer structure. And the weight and bulk of the jammer can be reduced dramatically. Therefore, this kind of jammer is especially suitable for distributed jamming, where multiple jammers are needed to be disposed within the to-be-protected area to extend the distribution of jamming and also to suppress the STAP anti-jamming measures.

APPENDIX A. DRFP WITH FAST-TIME MODULATIONS

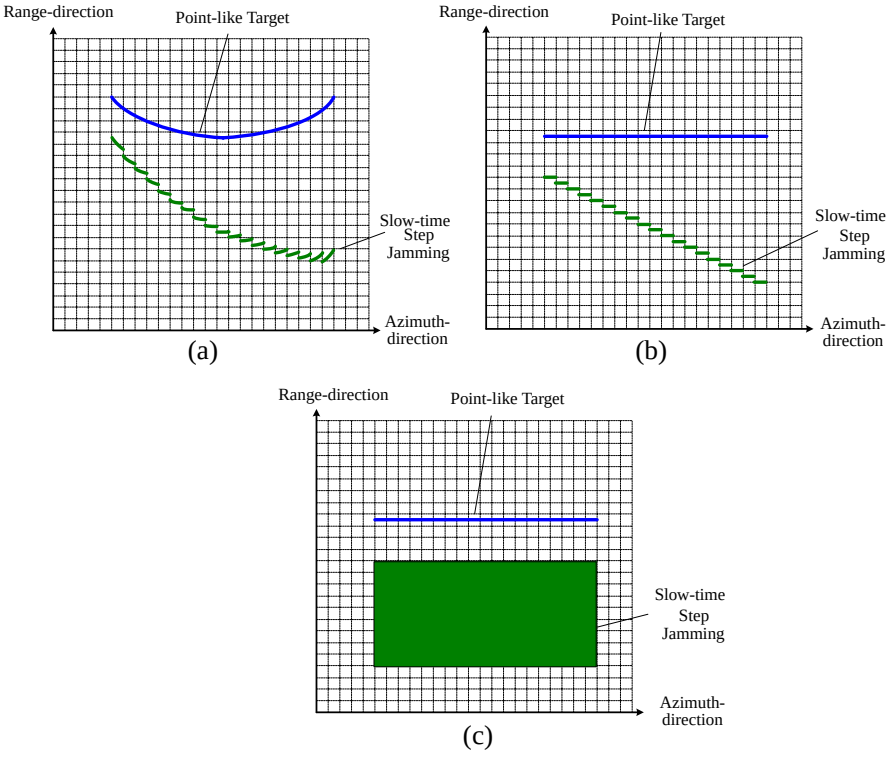

Figure A1. SAR imaging results of DRFP with stepped modulations in both directions. (a) SAR imaging after pulse compression in range-direction. (b) SAR imaging after RCMC. (c) SAR imaging after two-dimensional pulse compressions.

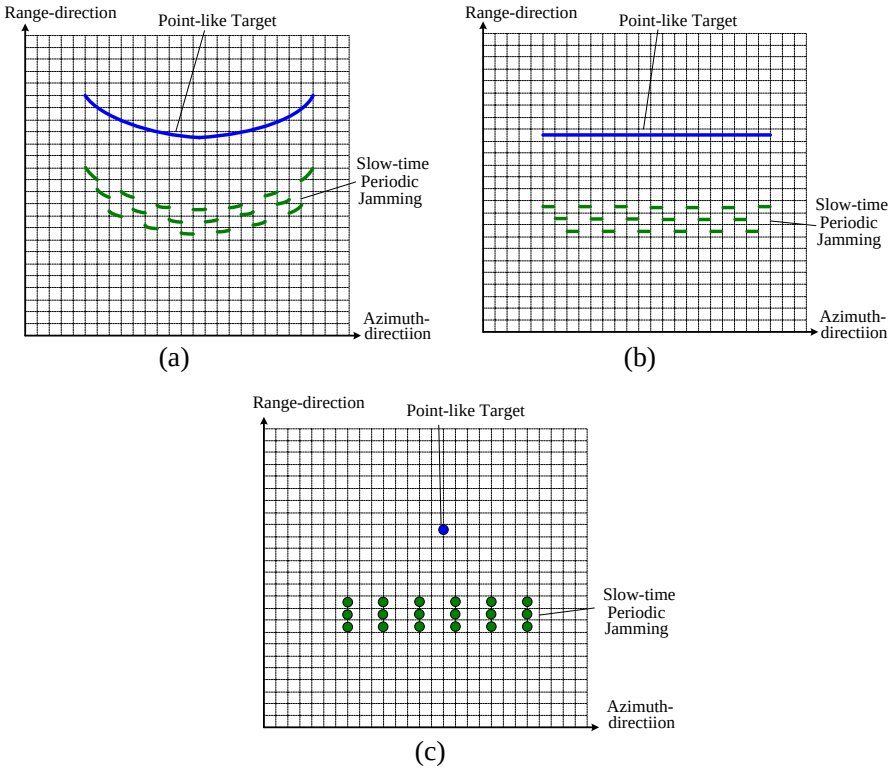

Figure A2. SAR imaging results of DRFP with periodic modulations in both directions. (a) SAR imaging after pulse compression in range-direction. (b) SAR imaging after RCMC. (c) SAR imaging after two-dimensional pulse compressions.

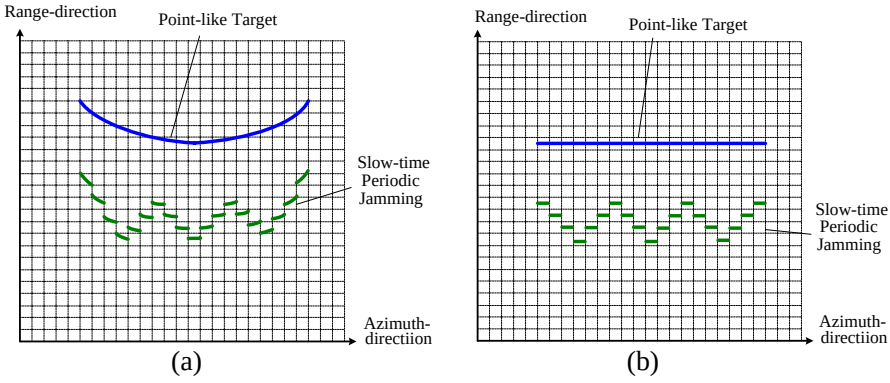

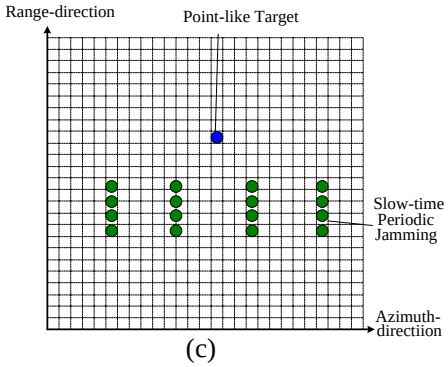

Figure A3. SAR imaging results of DRFP with grouped modulations in both directions. (a) SAR imaging after pulse compression in range-direction. (b) SAR imaging after RCMC. (c) SAR imaging after two-dimensional pulse compressions.

REFERENCES

1. Peng, X., W. Tan, Y. Wang, W. Hong, and Y. Wu, "Convolution back-projection imaging algorithm for downward-looking sparse linear array three dimensional synthetic aperture radar," *Progress In Electromagnetics Research*, Vol. 129, 287–313, 2012.
2. Koo, V. C., Y. K. Chan, V. Gobi, M. Y. Chua, C. H. Lim, C.-S. Lim, C. C. Thum, T. S. Lim, Z. bin Ahmad, K. A. Mahmood, M. H. Bin Shahid, C. Y. Ang, W. Q. Tan, P. N. Tan, K. S. Yee, W. G. Cheaw, H. S. Boey, A. L. Choo, and B. C. Sew, "A new unmanned aerial vehicle synthetic aperture radar for environmental monitoring," *Progress In Electromagnetics Research*, Vol. 122, 245–268, 2012.
3. Mohammadpoor, M., R. S. A. Raja Abdullah, A. Ismail, and A. F. Abas, "A circular synthetic aperture radar for on-the-ground object detection," *Progress In Electromagnetics Research*, Vol. 122, 269–292, 2012.
4. Zhou, W., J. T. Wang, H. W. Chen, and X. Li, "Signal model and moving target detection based on mimo synthetic aperture radar," *Progress In Electromagnetics Research*, Vol. 131, 311–329, 2012.
5. Lim, S. H., C. G. Hwang, S. Y. Kim, and N. H. Myung, "Shifting MIMO SAR system for high-resolution wide-swath imaging," *Journal of Electromagnetic Waves and Applications*, Vol. 25, Nos. 8–9, 1168–1178, 2011.

6. Xing, S., D. Dai, Y. Li, and X. Wang, "Polarimetric SAR tomography using $L_{2,1}$ mixed norm sparse reconstruction method," *Progress In Electromagnetics Research*, Vol. 130, 105–130, 2012.
7. Liu, Q. F., S. Q. Xing, X. S. Wang, and J. Dong, "A strip-map SAR coherent jammer structure utilizing periodic modulation technology," *Progress In Electromagnetics Research B*, Vol. 28, 111–128, 2011.
8. Liu, Q. F., S. Q. Xing, X. S. Wang, and J. Dong, "The interferometry phase of InSAR coherent jamming with arbitrary waveform modulation," *Progress In Electromagnetics Research*, Vol. 124, 101–118, 2012.
9. Liu, Q. F., S. Q. Xing, X. S. Wang, and J. Dong, "The 'slope' effect of coherent transponder in InSAR DEM," *Progress In Electromagnetics Research*, Vol. 126, 125–133, 2012.
10. Condley, C. J., "Some system considerations for electronic countermeasures to synthetic aperture radar," *IEE Colloquium on Electronic Warfare Systems,* 1–7, 1990.
11. Dumper, K., P. S. Cooper, A. F. Wons, C. J. Condley, and P. Tully, "Spaceborne synthetic aperture radar and noise jamming," *Proceeding IEE Radar*, 411–414, 1997.
12. Mrstik, V., "Agile-beam synthetic aperture radar opportunities," *IEEE Trans. on AES*, Vol. 34, No. 2, 500–507, Apr. 1998.
13. Ender, H. G., P. Berens, A. R. Brenner, et al., "Multi channel SAR/MTI system development at FGAN: From AER to PAMIR," *2002 IEEE International Geoscience and Remote Sensing Symposium*, Vol. 3, 1697–1701, 2002.
14. Paine, A. S., "An adaptive beamforming technique for countering synthetic aperture radar (SAR) jamming threats," *2007 IEEE Radar Conf.*, 630–634, 2007.
15. Wu, X. F., D. H. Dai, and X. S. Wang, "Study on SAR jamming measures," *IET International Conference on Radar Systems*, 176–179, Edinburgh, England, 2007.
16. Wu, X. F., D. H. Dai, X. S. Wang, and H. Z. Lu, "Evaluation of SAR jamming performance," *MAPE2007*, 1476–1479, Hangzhou, 2007.
17. Dai, D. H., X. F. Wu, X. S. Wang, and S. P. Xiao, "SAR active-decoys jamming based on DRFM," *IET International Conference on Radar Systems*, 1–4, 2007.